

MICROCOPY RESOLUTION TEST CHART
NATIONAL BUREAU OF STANDARDS-1963-A

12

AD-A133 846

TECHNICAL REPORT NO. 22

TO

THE OFFICE OF NAVAL RESEARCH
CONTRACT No. N00014-76-C-0037, NR 031-756

HYDROGEN EMBRITTLEMENT OF TITANIUM SHEET
UNDER MULTIAXIAL DEFORMATION PATHS

R. J. BOURCIER AND D. A. KOSS

DEPARTMENT OF METALLURGICAL ENGINEERING
MICHIGAN TECHNOLOGICAL UNIVERSITY
HOUGHTON, MI 49931

DTIC
ELECTE
OCT 21 1983
S B

DTIC FILE COPY

REPRODUCTION IN WHOLE OR IN PART IS PERMITTED FOR ANY PURPOSE
OF THE UNITED STATES GOVERNMENT. DISTRIBUTION OF THIS DOCUMENT
IS UNLIMITED.

DISTRIBUTION STATEMENT A
Approved for public release
Distribution Unlimited

| REPORT DOCUMENTATION PAGE | | READ INSTRUCTIONS BEFORE COMPLETING FORM |
|--|--|---|
| 1. REPORT NUMBER No. 22 | 2. GOVT ACCESSION NO. AD-A133 846 | 3. RECIPIENT'S CATALOG NUMBER |
| 4. TITLE (and Subtitle) Hydrogen Embrittlement of Titanium Sheet Under Multiaxial Deformation Paths | 5. TYPE OF REPORT & PERIOD COVERED | |
| | 6. PERFORMING ORG. REPORT NUMBER | |
| 7. AUTHOR(s) R. J. Bourcier and D. A. Koss | 8. CONTRACT OR GRANT NUMBER(s) N00014-76-C-0037 NR 031-756 | |
| 9. PERFORMING ORGANIZATION NAME AND ADDRESS Department of Metallurgical Engineering Michigan Technological University Houghton, MI 49931 | 10. PROGRAM ELEMENT, PROJECT, TASK AREA & WORK UNIT NUMBERS | |
| 11. CONTROLLING OFFICE NAME AND ADDRESS Office of Naval Research 800 N. Quincy Street Arlington, VA 22217 | 12. REPORT DATE August 1983 | |
| | 13. NUMBER OF PAGES | |
| 14. MONITORING AGENCY NAME & ADDRESS (if different from Controlling Office) | 15. SECURITY CLASS. (of this report) Unclassified | |
| | 15a. DECLASSIFICATION/DOWNGRADING SCHEDULE | |
| 16. DISTRIBUTION STATEMENT (of this Report) Distribution of this document is unlimited. | | |
| <div style="border: 1px solid black; padding: 5px; display: inline-block;"> DISTRIBUTION STATEMENT A Approved for public release; Distribution Unlimited </div> | | |
| 17. DISTRIBUTION STATEMENT (of the abstract entered in Block 20, if different from Report) | | |
| 18. SUPPLEMENTARY NOTES | | |
| 19. KEY WORDS (Continue on reverse side if necessary and identify by block number) Hydrogen Embrittlement, Titanium, Multiaxial States of Stress | | |
| 20. ABSTRACT (Continue on reverse side if necessary and identify by block number) The ductility of commercially pure titanium sheet containing either 60, 630, or 980 wt ppm hydrogen has been investigated over deformation paths ranging from uniaxial to equibiaxial tension. Based on measurements of fracture strains measured locally from grids, the data show a decrease in ductility with increasing hydrogen content as the degree of biaxiality of the tensile strain increases. Thus hydrogen embrittlement of Ti sheet depends on deformation path, being the most severe under equibiaxial straining. | | |

20. ABSTRACT (contd)

The embrittlement occurs even though hydrogen has no significant effect on the room temperature yielding and flow behavior of Ti in either uniaxial or balanced biaxial tension. Quantitative metallography indicates that void nucleation is due to hydride fracture and occurs at comparatively small strains in plane strain and equibiaxial deformation. An analysis shows that the strain-induced fracture of the hydrides appears to obey a critical normal stress criterion, the stresses being caused by: (a) the inhomogeneity of strain between the matrix and the particles and (b) the maximum principal stress within the matrix. Calculations show that only the latter changes significantly with loading path, and this is primarily due to the strong degree of plastic anisotropy in the Ti sheet. Furthermore, the void link-up process in equibiaxial tension initiates at a relatively low bulk void density, probably as a result of a localized plastic instability process. Thus, the susceptibility of titanium sheet to hydrogen embrittlement is most severe under those loading conditions which result in large normal stresses and which favor an accelerated link-up of voids created by the strain-induced fracture of hydrides.

| | |
|--------------------|---------|
| Accession | |
| NTIS | ✓ |
| DTIC | |
| Uncl | |
| Spec | |
| By | |
| Distribution | |
| Availability Codes | |
| Dist | Special |
| A | |

DTIC
COPY
INSPECTED
2

HYDROGEN EMBRITTLEMENT OF TITANIUM SHEET
UNDER MULTIAXIAL DEFORMATION PATHS

R. J. Bourcier and D. A. Koss
Department of Metallurgical Engineering
Michigan Technological University
Houghton, Michigan 49931

ABSTRACT

The ductility of commercially pure titanium sheet containing either 60, 630, or 980 wt ppm hydrogen has been investigated over deformation paths ranging from uniaxial to equibiaxial tension. Based on measurements of fracture strains measured locally from grids, the data show a decrease in ductility with increasing hydrogen content as the degree of biaxiality of the tensile strain increases. Thus hydrogen embrittlement of plastically anisotropic Ti sheet depends on deformation path, being the most severe under equibiaxial straining. The embrittlement occurs even though hydrogen has no significant effect on the room temperature yielding and flow behavior of Ti in either uniaxial or balanced biaxial tension. Quantitative metallography indicates that void nucleation is due to hydride fracture and occurs at comparatively small strains in plane strain and equibiaxial deformation. An analysis shows that the strain-induced fracture of the hydrides appears to obey a critical normal stress criterion, the stresses being caused by (a) the inhomogeneity of strain between the matrix and the particles and (b) the maximum principal stress within the matrix. Calculations show that only the latter changes significantly with loading path, and this is primarily due to the strong degree of plastic anisotropy in the Ti sheet. Furthermore, the void link-up process in equibiaxial tension initiates at a relatively low bulk void density, probably as a result of a localized plastic instability process. Thus, the susceptibility of titanium sheet to hydrogen embrittlement is most severe under those loading conditions which result in large normal stresses and which favor an accelerated link-up of voids created by the strain-induced fracture of hydrides.

INTRODUCTION

Although commercially pure (C.P.) titanium can be embrittled by hydrogen, the degree of embrittlement has been observed to depend on many factors. For example, smooth bar specimens tested at slow strain rates in uniaxial tension usually show relatively little signs of embrittlement at levels of hydrogen up to wt. 400 ppm [1-3]. On the other hand, substantial embrittlement at similar hydrogen contents occurs in bar or plate material upon the introduction of notches, decreasing the test temperature, and increasing the strain-rate, oxygen content, or grain size [1-6]. Metallographic evidence indicates that these embrittlement effects are associated with the introduction of cracks into the titanium matrix by the local fracture of titanium hydride precipitates [2,3].

In recent years, there has been an increasing demand for C.P. Ti sheet or tubing products. Although the sheet and tubing typically are loaded in service under multiaxial states of stress and will deform under conditions of plane stress, the hydrogen embrittlement of C.P. Ti under these conditions has not been characterized. The previous results on notched tensile or impact specimens indicate that embrittlement can occur in thick section components under conditions of a large hydrostatic stress [1,4,6]. However, such a stress state is local to the tip of the notch, difficult to characterize in a deforming body, and has a degree of triaxiality (as measured by the hydrostatic stress/equivalent shear stress ratio) which is four to five times greater than that possible even in the equibiaxial tension of smooth sheet or thin wall tubing. Utilizing the techniques of punch-stretch testing applied to hydrogen embrittlement [7], this study investigates the embrittlement of C.P. Ti sheet at three levels of hydrogen content (60, 630, and 980 wt ppm) and deformed over a range of multiaxial strain paths from uniaxial tension to

balanced biaxial tension. Quantitative metallography and fractography will be correlated with the mechanical properties, and the observed dependence of hydrogen embrittlement on multiaxial loading path will be examined in terms of existing theories of ductile fracture.

EXPERIMENTAL PROCEDURE

The material used in this study consists of 0.75 mm thick C.P. Ti (Ti-50A) sheet kindly supplied by TIMET Corp. After the heat treatments described below, the sheet had a grain size of 0.015 mm and contained 1460 wt ppm oxygen. The crystallographic texture of specimens also after heat treatment is typical of C.P. Ti [8] and is shown in Fig. 1.

Hydrogen was thermally charged into the test specimens using a modified Sieverts apparatus. The specimens to be charged were first annealed under a dynamic vacuum of $\sim 1.3 \times 10^{-6}$ kPa at 973K for 30 minutes. At that point, the system was isolated and a measured amount of hydrogen gas was introduced; a rapid pressure drop indicated almost immediate adsorption onto the Ti sheet. After allowing the hydrogen to diffuse for 45 minutes at 973K, the specimens were cooled to room temperature at an average rate of ~ 73 K/minute. Uncharged ("annealed") sheet was subjected to the same heat treatment as the charged material except that the system was always under dynamic vacuum; no hydrogen was introduced. After heat treatment/charging, the sheet specimens contained either 60, 630, or 980 wt. ppm hydrogen.

The microstructures of the annealed and hydrogen-charged sheet material are shown in Fig. 2. The 60 ppm H material shows little or no evidence of hydrides and only a small amount of retained beta phase, which is the equiaxed darker constituent. The 630 ppm H material contains many hydride platelets roughly 12 μm long x 0.8 μm wide occurring both trans- and intergranularly. The 980 ppm H heat shows a much coarser hydride structure with platelets ~ 25

μm long x $2.5 \mu\text{m}$ wide occurring primarily along grain boundaries. These platelets show a substantial degree of branching and interconnectedness.

The mechanical tests have been based on the techniques developed by Hecker for sheet metal formability studies [9,11] and applied to hydrogen embrittlement by Bourcier and Koss [7]. All testing was performed at room temperature, usually at an average engineering strain rate of $2 \times 10^{-3} \text{ s}^{-1}$, although some tensile tests were also conducted at $8 \times 10^{-5} \text{ s}^{-1}$. Punch-stretch testing utilized a 50 mm hemispherical punch; the apparatus and procedure have been described elsewhere [7]. In all cases, the specimens were photogridded with either 1.27 mm diameter contacting circles or 0.50 mm squares in order to determine the strain on a local basis. Local grid strains were measured from individual 1.27 mm circles or 2x2 regions of 0.50 mm square grids. The fracture strain data presented in this study have been determined by directly measuring ϵ_1 and ϵ_2 from strained grid elements spanning the fracture surface. An alternate method of measuring a value of the fracture strain is to measure the width strain ϵ_2 of a grid element at the fracture surface and the thickness strain ϵ_3 from the thickness profile at that grid element and to calculate (using $\epsilon_1 + \epsilon_2 + \epsilon_3 = 0$) the value of ϵ_1 at fracture. This latter technique avoids the problem of strain gradients which exist along an element of material near fracture, but the resulting values of ϵ_3 usually exhibit considerable scatter due to the irregularity of the specimen thickness along the fracture surface (given the scale of the sheet thickness, small irregularities result in large scatter in thickness strain). Also, the assumption of conserved volume is not strictly valid for a cavitating material.

EXPERIMENTAL RESULTS

The effect of internal hydrogen on the uniaxial tensile behavior of the C.P. Ti sheet is illustrated in Fig. 3. From this data, it may be

concluded that at the relatively low strain rate of $2 \times 10^{-3} \text{ s}^{-1}$, hydrogen exerts only minor influences on the uniaxial tensile properties of C.P. Ti sheet. Increasing hydrogen content causes a small decrease in the strain hardening exponent n obtained by fitting the stress-strain ϵ curves to the $\sigma = k\epsilon^n$ relationship in the strain range $0.01 < \epsilon < 0.10$. In addition, H causes a slight decrease in tensile ductility as measured either by the reduction in area or the strain to failure as determined locally from the grid elements spanning the fracture surface. These data are consistent with earlier uniaxial tension results [1-3].

Close inspection of the data in Fig. 3 shows in fact that the mechanical parameters of the textured Ti sheet are more strongly dependent on sample orientation than on hydrogen content. This is a result of the large degree of plastic anisotropy exhibited by the sheet. Using the parameters R and P to define plastic anisotropy (where in this case R and P are $\epsilon_{\text{width}}/\epsilon_{\text{thickness}}$ in tensile tests of specimens parallel to either the rolling direction (R) or the transverse direction (P)), the tests show $R \approx 2.2$ at all levels of H and $P = 5.5$ at 60 ppm H, 4.9 at 630 ppm H, and 4.6 at 980 ppm H.

The influence of multiaxial deformation path on the hydrogen embrittlement of the C.P. Ti sheet is shown in Fig. 4, which is a fracture limit diagram identifying at failure the major or minor principal strains (ϵ_1 and ϵ_2 , respectively) in the plane of the sheet.* The fracture strains in Fig. 4 have been obtained from measurements of fractured grid elements, which exhibit better reproducibility of data than do those obtained from thickness strain determination (see Experimental Procedure section). Data based on the thickness strain technique shows similar curves to those in Fig. 4 but with

*Fig. 4 should not be confused with the "forming limit diagram" which identifies the onset of localized necking of sheet in ϵ_1 - ϵ_2 space [9-11]. In this study fracture of the hydrided sheet occurs prior to the onset of localized necking, regardless of strain path.

the data displaced to larger values of ϵ_1 by increments of $\Delta\epsilon=0.05$ (at 980 ppm H) to $\Delta\epsilon_1=0.10$ (at 60 ppm H). Finally it might be noted that, for each hydrogen level tested, failure at $\epsilon_2 \leq 0$ in Fig. 4 is limited by fracture perpendicular to the transverse direction of the sheet. In equibiaxial stretching, the Ti-60H sheet failed after localized necking perpendicular to the rolling direction. In contrast, the Ti-630H and Ti-980H sheets, which did not form necks, also did not show any orientation dependence of the fracture plane with respect to the rolling direction when tested in equibiaxial tension.

The fracture limit diagram in Fig. 4 shows the susceptibility of C.P. Ti sheet to hydrogen embrittlement for nearly all deformation paths which result in sheet thinning. The most striking feature of these curves is the decrease in ductility with increasing hydrogen content as the degree of biaxiality of the tensile strain increases. Thus, hydrogen embrittlement in C.P. Ti sheet depends on the multiaxial deformation path, being the greatest under conditions of equibiaxial tension. An illustration of this effect is shown in Fig. 5 in which the normalized equivalent strain to failure, $\bar{\epsilon}_f$, has been calculated using the data in Fig. 4, the measured R- and P-values reported earlier, and Hill's original, quadratic yield criterion [12] which provides an adequate description of the multiaxial stress-strain behavior of C.P. Ti containing H [13]. Fig. 5 clearly indicates that the Ti sheet exhibits virtual immunity to hydrogen embrittlement in uniaxial tension while the ductility is decreased a factor of 2.5 in equibiaxial tension. Visual observations of the test specimens also provide a striking contrast of influence of hydrogen on the uniaxial vs. balanced biaxial tensile behavior of the C.P. Ti sheet (for example, see ref. 7).

It is well established that the hydrogen embrittlement of Ti and its alloys is associated with the formation of titanium hydrides. In the case

of titanium, the hydrides fracture introducing cracks and voids into the matrix [2,3]. An example of such a process in the Ti at high hydrogen contents is shown in Fig. 6 in which titanium hydrides have fractured and nucleated voids. In uniaxial tension, most of the hydrides visible near the fracture surface appear to be aligned roughly parallel to the tensile axis and are fractured along their length as in Fig. 6a. Under balanced biaxial tension as shown in Fig. 6b, the hydrided material again is characterized by voids associated with the fracture of the hydride platlets as well as a small number of voids formed by hydride-matrix interfacial decohesion. In equibiaxial tension, no preferential alignment of fractured hydrides is evident, and all orientations of hydrides appear equally prone to failure.

In contrast to the above observations, the Ti-60 H exhibits relatively little void formation beneath the fracture surface. Even in this material, most of the voids are associated with very small (5 μm long) plate-like second phase particles which occur in the highly strained regions near the fracture surface. Under biaxial tension, the 60 ppm H material again shows a very low void density near the fracture surface, but substantially more small, plate-like second phase particles are present near the fracture surface.

The critical equivalent strain $\bar{\epsilon}_N$ necessary to nucleate a "significant" void density of 10^2 voids/ mm^2 has also been obtained by the combination of dark field quantitative optical microscopy and strain gradient measurements as a function of position along a deformed specimen.* The nucleation strains estimated here are microscopic values and do not indicate the particular strain condition for individual particles; these will fracture over a range of strains depending on factors such as particle size, shape, orientation,

*A void density of 10^2 voids/ mm^2 corresponds to an area fraction of voids of 3×10^{-4} , given an average void size of 2 μm diameter. Alternatively, at 1000X there is one void in an area 10cm x 10cm.

location, and internal flaws. Based on voids $\geq 1 \mu\text{m}$ in diameter being resolved, Fig. 7a shows the results of such measurements with $\bar{\epsilon}_N$ being normalized to the critical strain to fracture $\bar{\epsilon}_f$ in Fig. 7b. Fig. 7 thus shows, on a comparative basis, the ease of void formation in Ti for the different deformation paths and hydrogen levels examined. As H content increases, void nucleation occurs at smaller strains for all strain paths; however, the decrease of ϵ_N with increasing H content is the largest in equibiaxial tension as seen in Fig. 7a. In distinct contrast to uniaxial tension behavior, fracture of the sheet in plane strain and equibiaxial tension at all H contents occurs soon after the significant void density is detected (i.e., $\bar{\epsilon}_N/\bar{\epsilon}_f \approx 0.95$); see Fig. 7b. It is interesting to note in Fig. 7 that in uniaxial tension no significant loss of ductility occurs (Fig. 5) despite the decrease in $\bar{\epsilon}_N$ and $\bar{\epsilon}_N/\bar{\epsilon}_f$ with increasing H content.

Examination of test specimen fracture surfaces shows the influence of both stress state and hydrogen level, Fig. 8. Failure in the 60 ppm material (see Fig. 8a) appears to be essentially a process of void nucleation, growth, and coalescence. Changing the strain state from uniaxial toward balanced biaxial tension results in a fracture surface with a decreased dimple size and increasingly planar topography. While failure of the hydrided material also occurs in a ductile manner, there is a distinct difference in the fracture surface appearance. The dimpled microvoid fracture seen in the 60 ppm sheet is replaced in the hydrided material by an irregular surface showing regions of substantial microcracking and "brittle-like" features; see Fig. 8b. Changing the imposed stress state from uniaxial toward balanced biaxial tension in sheet containing 630 to 980 H yields a fracture surface with finer features, less surface relief, and facets which may be former hydride/matrix interfaces.

DISCUSSION

The most significant result of this study is the decrease in ductility with increasing internal hydrogen as the degree of biaxiality of the tensile strain increases (Figs. 4 and 5). Thus, hydrogen embrittlement in C.P. Ti sheet at low strain-rates depends on the multiaxial deformation path, and it is greatest at equibiaxial tension. The sensitivity of hydrogen embrittlement to multiaxial tension occurs in the absence of any large effect of hydrogen on the yield stress and strain hardening behavior of Ti in either uniaxial tension (Fig. 3) or the multiaxial deformation of tubes tested in combined tension and internal pressure [13].

As observed in previous studies of hydrogen embrittlement of Ti [2,3,5], the failure process in the sheet is by a ductile fracture process (Fig. 8) in which void formation is caused by the strain-induced fracture of hydrides (Fig. 6). In this case, ductile fracture may be divided into sequential stages of: (1) hydride fracture/void nucleation, (2) void growth, and (3) void link-up. While no observations have been made of void growth in the present study, Fig. 7a clearly shows that increasing hydrogen content accelerates void nucleation (i.e., $\bar{\epsilon}_N$ decreases with increasing H content for all strain paths). Plane strain deformation is clearly the most effective in nucleating voids while the decrease in $\bar{\epsilon}_N$ with increasing H content is especially pronounced in equibiaxial tension. In addition, Fig. 7b shows that fracture in both plane strain and equibiaxial tension occur at strains $\bar{\epsilon}_f$ which are only 5% greater than $\bar{\epsilon}_N$. Thus, insofar as the void link-up process is concerned, fracture occurs in both plane strain and equibiaxial deformation at a much lower bulk void density than in uniaxial tensile deformation. Therefore hydrogen embrittlement of Ti sheet in balanced biaxial tension is, at least in part, a consequence of (1) plane strain and equibiaxial tensile

deformation being especially effective in fracturing hydrides and forming voids (Fig. 7a) and (2) void link-up in equibiaxial tension being initiated at a relatively small density of voids (Fig. 7b).

The enhancement of hydride fracture by plane strain and equibiaxial deformation of sheet may be understood on the basis that hydride fracture obeys a maximum normal stress criterion. This is consistent with several analyses of the nucleation of cavities at large ($1 \mu\text{m}$) inclusions by plastic deformation [14-18]. Hydride fracture would thus be a result of local normal stresses imposed on the hydrides under conditions in which either (a) the strain in the hydride equals that in the matrix (fiber loading) or (b) there exists an inhomogeneity of strain between the plastically deforming matrix and the hydride. Fiber loading, which has been previously invoked as the source of local normal stresses to explain fracture of elongated carbides in steels [19], relies on the strain in an elongated particle being equal to that in the plastically deforming matrix. If the particle remains elastic, very large stresses ($=E \epsilon$, where E is the elastic modulus of the particle and ϵ is the matrix strain) are induced in the particle, being a maximum near the center of a particle orientated parallel to the maximum principal strain axis of the matrix. Given the large values of $\bar{\epsilon}_N$ observed in the present study ($\bar{\epsilon}_N > 0.2$), fiber loading concepts clearly indicate that the hydride particles in the present study must deform plastically prior to failure. If so, the stresses must be relatively uniform along most of the length of the hydrides. This is consistent with examinations of hydride fractures, such as in Fig. 6, which indicate that cracks are randomly situated along the length of the hydrides. However, given the difficulty of slip at room temperature in titanium hydrides in which bulk hydrides exhibit strains to failure of less than 0.03 in compression [20], it seems much more likely that there is an inhomogeneity of strain between the matrix and hydride. Furthermore, the

normal stresses responsible for particle failure in a fiber loading analysis are based on the matrix strain with the maximum fiber stress associated with the maximum principal strain within the matrix. As such, fiber loading cannot explain why plane strain deformation should be any more effective in fracturing hydrides than simple tension; Fig. 7 clearly shows that it is. Thus, we conclude that hydride failure must be associated with internal stresses developed within the hydride which, while relatively uniform along the length of the hydride, are due to an inhomogeneity of strain between the hydride and matrix.

The state of stress in the vicinity of a hard (usually spherical) particle embedded in a plastically deforming matrix has been studied extensively from the standpoint of void nucleation [14-18]. Of these analyses, that of Beremin [17], which is based on an extension of Eshelby's theory for inclusions [21] proposed by Berveiller and Zaoui [22], is the most appropriate for the present study in that it examines the stress state within plate-like particles which, while surrounded by a deforming matrix, may themselves also deform plastically. The stresses σ_{ij}^P within a particle deforming according to strain components ϵ_{kl}^P are given by [17,22]:

$$\sigma_{ij}^P = \sigma_{ij}^m + \frac{2}{3} \frac{\bar{\sigma}^m}{\bar{\epsilon}^m} (S_{ijkl}^{-1} - I_{ijkl}) (\epsilon_{kl}^m - \epsilon_{kl}^P) \quad (1)$$

where σ_{ij}^m and ϵ_{kl}^m are the stress and strain state respectively in the matrix, $\bar{\sigma}^m$ and $\bar{\epsilon}^m$ are the equivalent stress and strains in the matrix, and S_{ijkl}^{-1} and I_{ijkl} are respectively the Eshelby tensor [21] and a unit tensor. Eq. 1 may be evaluated assuming that the stresses and strains are homogeneous in the inclusion as well as in the matrix, that $d\bar{\sigma}^m/d\bar{\epsilon}^m$ is a constant and that the matrix-particle interaction is formulated from deformation theory of

plasticity. In the present study, it should be noted that the material is plastically anisotropic and we assume Hill's quadratic yield criterion and the associated flow rule. Strain gradients already exist near the hydride particles during their nucleation and growth because of the 20% size misfit of the hydrides [23], and additional stress/strain gradients will undoubtedly develop near the particles during deformation. Nonetheless, this analysis is the only one presently available capable of providing at least an approximate indication of the influence of multiaxial loading path on the stresses within hydrides which have a limited capacity to deform, have a plate-like shape, and have specified orientations with respect to the principal strain directions.

A complete evaluation of Eq. 1 requires knowledge of the relationship between deformation within the matrix and that within the particle (the $(\epsilon_{kl}^m - \epsilon_{kl}^p)$ tensor in Eq. 1). The maximum value of this tensor occurs when $\epsilon_{kl}^m \gg \epsilon_{kl}^p$, which occurs when deformation within the particle is limited. In this case, Beremin show that the equivalent strain to nucleate a void $\bar{\epsilon}_N$ by particle fracture at a critical internal stress σ_c is [17]

$$\bar{\epsilon}_N = (\lambda E_p)^{-1} [\sigma_c - \sigma_1] \quad (2)$$

where λ is a constant which depends on particle shape and strain path, $E_p = d\bar{\sigma}/d\bar{\epsilon}$ of the matrix and σ_1 is the maximum principal stress in the matrix. For a flat oblate spheroid (disc) with $a=b \gg c$ and $k=c/a \ll 1$, the maximum values of λ (the most effective condition for fracturing hydrides) may be estimated applying the Beremin analysis [17] to a plastically anisotropic material. The approximate values of λ are: $(-0.7 + 0.7/k)$, $(-0.4 + 0.5/k)$, or $(-0.2 + 0.4/k)$ for uniaxial tension, plane strain tension, or equibiaxial tension, respectively, for the range of plastic anisotropy encountered. Increasing

deformation within the particle will decrease these values of λ , although the exact expressions depend on the relationships between ϵ_{kl}^m and ϵ_{kl}^p .

The dependence of $\bar{\epsilon}_N$ on stress path and hydrogen content may now be examined in terms of eq. 2. The minimum values of $(\lambda E_p)^{-1}$ can be estimated assuming $\epsilon_{kl}^m \gg \epsilon_{kl}^p$, the values of E_p (1250 to 1725 MPa) based on multiaxial stress-strain behavior of Ti-1000ppmH [13], and the hydrides to be disc-shaped with $k = 0.07$ at 630H and $k = 0.10$ at 980H. For all deformation paths and both levels of hydrogen, $(\lambda E_p)^{-1} \geq (0.8 \text{ to } 1.6) \times 10^{-4} \text{ MPa}^{-1}$. Thus, so long as a given hydride is suitably oriented along the principal stress direction, the roughly constant value of $(\lambda E_p)^{-1}$ and Eq. 2 indicates a nearly equal probability of hydride failure independent of loading path at given value of σ_1 . Although the analysis shows that a greater proportion of hydrides in sheet undergoing plane strain and equibiaxial deformation experience large tensile stresses than in uniaxial tension, we conclude that the dependence of $\bar{\epsilon}_N$ on stress path does not occur because of any strong sensitivity of the $(\lambda E_p)^{-1}$ term.

Given the plastic anisotropy of the Ti sheet ($R = 2.2$ and $P = 4.9 - 4.6$ at 630 and 980H, resp.), the maximum principal stress σ_1 term in eq. 2 is not constant but varies considerably with loading path from $\sigma_1 = 1.0\bar{\sigma}$ in uniaxial tension (RD) to $\sigma_1 = 1.47\bar{\sigma}$ in equibiaxial tension and $\sigma_1 = 1.66\bar{\sigma}$ in plane strain (TD) tension.* A dependence of $\bar{\epsilon}_N$ on σ_1 results from varying the strain path causing the dependence shown in Fig. 9. As shown, there is reasonable agreement between the predicted form of Eq. 2 and the observed results. In particular, minimum and maximum values of $\bar{\epsilon}_N$ (plane strain and uniaxial tension (TD) respectively) are correctly predicted. The data in Fig.

*The values of σ_1 at $\bar{\epsilon} = \bar{\epsilon}_N$ can be estimated using uniaxial stress-strain data, Hills quadratic yield criterion [12], and isotropic strain hardening, noting multiaxial σ - ϵ behavior of Ti obeys these assumptions well [13].

9 may be used to obtain an experimental value of $(\lambda E^P)^{-1}$. This exceeds the minimum values predicted (0.8 to $1.6 \times 10^{-4} \text{ MPa}^{-1}$) by a factor of about 4, which is consistent with a considerable plastic strain occurring in the hydrides. A rough estimate of hydride plastic strain can be obtained by assuming that the strains between hydrides and matrix are proportional; thus, $\epsilon_{kl}^P \approx \frac{3}{4} \epsilon_{kl}^m$ would be consistent with the present results. Finally, it should be noted that Fig. 9 indicates that $\sigma_c \approx 1210 \text{ MPa}$ for the larger hydrides in the Ti-980H and 1380 MPa for the hydrides in the Ti-630H. This is consistent with the notion of larger particles having a high probability of containing a flaw.

We therefore conclude that the effectiveness of plane strain and equibiaxial deformation in fracturing the titanium hydrides and nucleating voids can be understood on the basis of a critical normal stress criterion for hydride fracture. According to our estimates, the stress component $(\alpha \lambda E_p)$ created by the inhomogeneity of strain between the matrix and particle is not very sensitive to deformation path. However, given the plastic anisotropy of the Ti sheet ($R = 2.2$ and $P \approx 4.6 - 4.9$), the maximum principal stress within the matrix is quite sensitive to deformation path, and it is this stress component which appears to be primarily responsible for the effectiveness of plane strain and equibiaxial deformation in fracturing the hydrides.

There are also factors which favor the onset of void coalescence at a small void density in equibiaxial tension when compared to uniaxial tension. First, given that the hydrostatic stress in balance biaxial tension is twice that in uniaxial tension the rate of void growth per unit strain in equibiaxial tension should exceed that in uniaxial tension [24,25]. Thus at a given strain, there should be more large voids in equibiaxial tension. This will clearly favor coalescence and tend to increase the $\bar{\epsilon}_N / \bar{\epsilon}_f$ ratio in Fig. 7b. Results from a study of the hydrogen embrittlement of Zircaloy-2

sheet confirm the void growth rates are much greater in equibiaxial tension than in uniaxial tension with the growth rates being independent of hydrogen content [26].

A second factor favoring the rapid onset of void link-up in equibiaxial tension is that in the hydrided material, void link-up appears to occur not solely by the impingement of growing voids but rather that the hydrides themselves participate in the link-up stage. The fracture surface no longer consists of well-defined dimples, as in Figs. 8a and 8b, but a more irregular surface occurs (Figs. 8c and 8d) as some of the voids link-up by failure within the plate-like hydrides or along the hydride-matrix interface. Such a link-up process is initiated in plane strain and equibiaxial tension at comparatively low void densities as evidenced by failure occurring rapidly after the 100 voids/mm² "nucleation density" of voids is detected. As a result, $\bar{\epsilon}_N/\bar{\epsilon}_f \approx 0.95$ for both plane strain and equibiaxial tension (Fig. 7b). This sensitivity to a small void density suggests that failure in plane strain and equibiaxial tension, regardless of hydrogen content, may occur due a local plastic instability process which creates locally large strains. These large local strains would account for the high density ($\sim 1000/\text{mm}^2$) of small dimples on the fracture surfaces at 60 H (Fig. 8b) and for enhancing void link-up via hydride failure at 630 and 980 H (Fig. 8d). In contrast, the ratios of $\bar{\epsilon}_N/\bar{\epsilon}_f$ in uniaxial tension are much lower ($0.55 \leq \bar{\epsilon}_N/\bar{\epsilon}_f \leq 0.75$) and metallography shows that the void density increases continuously (to $\sim 250/\text{mm}^2$) as the fracture surface is approached. Thus deformation in uniaxial tension "tolerates" a higher void density, probably because it is more resistant to the plastic instability process which appears to cause final separation of the fracture surfaces by massive void link-up.

SUMMARY

The most significant observation of this study is the sensitivity of hydrogen embrittlement of Ti sheet to deformation path. Specifically there is a large loss of ductility at high H contents in equibiaxial tension even though a negligible loss of ductility occurs in uniaxial tension. This form of hydrogen embrittlement can be understood in the context of a ductile fracture process in which hydrides undergo strain-induced fracture and form voids. The strain to nucleate a significant density of voids (10^2 voids/mm²) decreases with increasing hydrogen content (and increased size of hydrides), and it is much smaller in plane strain and equibiaxial tension than in uniaxial tension. Thus, equibiaxial and plane strain tensile deformation are especially effective in fracturing hydrides. This effect can be understood in terms of a critical normal stress criterion for hydride fracture. An approximate analysis shows that the normal stresses within plate-like particles are the sum of two components: (1) a stress due to the inhomogeneity of strain between the particles and matrix, and (2) the maximum principal stress within the matrix. Only the latter component is very sensitive to the deformation path, varying in this study from $1.0\bar{\sigma}$ in uniaxial tension (RD) to $1.66\bar{\sigma}$ in plane strain tension (TD) because of the plastic anisotropy ($R=2.2$ and $P=4.6-5.2$) inherent in the sheet. Once voids have formed, the mechanics of the failure process under multiaxial deformation are such that the void link-up begins at a comparatively low density of voids in plane strain and equibiaxial deformation. This appears to be a consequence of the onset of a local plastic instability process which rapidly links the hydride-induced voids present and which occurs at small void densities in plane strain and equibiaxial tension.

ACKNOWLEDGEMENTS

The authors are grateful to Dr. H. Rosenberg and TIMET Corporation for kindly supplying the material used in this study. This research was supported by the Office of Naval Research through Contract No. N00014-76-0037, NR031-76.

LIST OF FIGURES

- Fig. 1 - Basal and prism pole figures of the titanium sheet material tested. The numbers indicate the relative intensities of the poles in number of times random.
- Fig. 2 - Optical micrograph showing titanium sheet containing (a) 60 ppm H, (b) 630 ppm H, and (c) 980 ppm H.
- Fig. 3 - The influence of hydrogen content on the (a) yield and tensile strength, (b) strain hardening exponent m , and strain-rate hardening exponent, m , and (c) the local fracture strain. All data are from uniaxial tensile tests of specimens either parallel to the rolling direction RD or transverse to the rolling direction TD.
- Fig. 4 - A fracture limit diagram showing the major ϵ_1 and minor ϵ_2 principal strains in the plane of the sheet at fracture. Data is for Ti containing three levels of hydrogen and tested over a range of deformation paths.
- Fig. 5 - The influence of hydrogen content on the equivalent strain at fracture $\bar{\epsilon}_f$ of titanium deforming in either uniaxial tension (transverse to the rolling direction), equibiaxial tension, or plane strain tension.
- Fig. 6 - Electron micrographs showing strain-induced hydride fracture and void formation in (a) uniaxial tension and (b) equibiaxial tension.
- Fig. 7 - The influence of hydrogen on (a) the equivalent strain $\bar{\epsilon}_N$ required to form 10^2 voids/mm² and (b) ratio of $\bar{\epsilon}_N$ to the equivalent strain at fracture $\bar{\epsilon}_f$. The terms TD and RD refer to uniaxial tensile deformation in the transverse and rolling directions, respectively while B/B and P denote balanced biaxial and plane strain tension, respectively.
- Fig. 8 - Electron micrographs showing the fracture surfaces the following specimens: (a) Ti-60 H deformed in uniaxial tension, (b) Ti-60 H deformed in equibiaxial tension, (c) Ti-980 H deformed in uniaxial tension, and (d) Ti-980 H deformed in equibiaxial tension.
- Fig. 9 - The dependence of the void nucleation strain $\bar{\epsilon}_N$ on the maximum principal stress σ_1 within the matrix at a plastic strain $\bar{\epsilon} = \bar{\epsilon}_N$.

REFERENCES

1. R. I. Jaffee, G. A. Lenning, and C. M. Craighead, *Trans. Met. Soc. AIME* 206, 907 (1956).
2. C. J. Beevers, M. R. Warren, and D. V. Edmonds, *J. Less-Common Metals* 14, 387 (1968).
3. C. J. Beevers and D. V. Edmonds, *Trans. Met. Soc. AIME* 245, 2391 (1969).
4. G. A. Lenning, C. M. Craighead, and R. I. Jaffee, *Trans. Met. Soc. AIME* 200, 367 (1954).
5. M. Nishigaki, A. Tanabe, Y. Ito, and Y. Moriguchi, in Titanium '80, Science and Technology, (edited by H. Kimura and O. Izumi), p. 1663 TMS-AIME, Warrendale, PA (1980).
6. K. J. Puttlitz and A. J. Smith in Hydrogen Effects in Metals (edited by I. M. Bernstein and A. W. Thompson), p. 427, TMS-AIME, Warrendale, PA, 1981.
7. R. J. Bourcier and D. A. Koss, *Scripta Met.* 16, 515 (1982).
8. F. Larson and A. Zarkades, Properties of Textures Titanium Alloys, Metals and Ceramics Information Center, Battelle, Columbus, OH, 1974.
9. S. S. Hecker, *Met. Eng. Quart.* 16, 30 (1974).
10. S. S. Hecker, *Sheet Metal Industries* 671 (1975).
11. A. K. Ghosh and S. S. Hecker, *Metall. Trans A* 6A, 1065 (1975).
12. R. Hill, The Mathematical Theory of Plasticity, p. 318, Oxford Press (1950).
13. C. W. Lentz, D. A. Koss, M. G. Stout, and S. S. Hecker, *Metall. Trans* (in print).
14. K. Tanaka, T. Mori, and T. Nakamura, *Phil. Mag.* 21, 267 (1970).
15. A. S. Argon, J. Im., and R. Satoglu, *Metall. Trans. A* 6A, 825 (1975).
16. S. H. Goods and L. M. Brown, *Acta Met.* 217, 1 (1979).
17. F. M. Beremin, *Metall. Trans A* 12A, 723 (1981).
18. G. LeRoy, J. D. Embury, G. Edward, and M. F. Ashby, *Acta Met.* 29, 1509 (1981).
19. T. C. Lindley, G. Oates, and C. E. Richards, *Acta Met* 18, 1127 (1970).
20. P. E. Irving and C. J. Beevers, *J. Mat'l. Sci.* 7, 23 (1972).
21. J. D. Eshelby, *Proc. Roy. Soc.* A241, 376 (1957).
22. M. Berveiller and A. Zaoui, *J. Mech. Phys. Solids* 26, 325 (1979).

23. N. E. Paton and J. C. Williams in Hydrogen in Metals (edited by I. M. Bernstein and A. W. Thompson), p. 409, AM. Soc. Met., Metals Park, OH (1974).
24. F. A. McClintock, J. Appl. Mech. 35, 363 (1968).
25. J. R. Rice and D. M. Tracey, J. Mech. Phys. Solids 17, 201 (1969).
26. Fan Yunchang and D. A. Koss, unpublished research, Michigan Technological University, 1983.

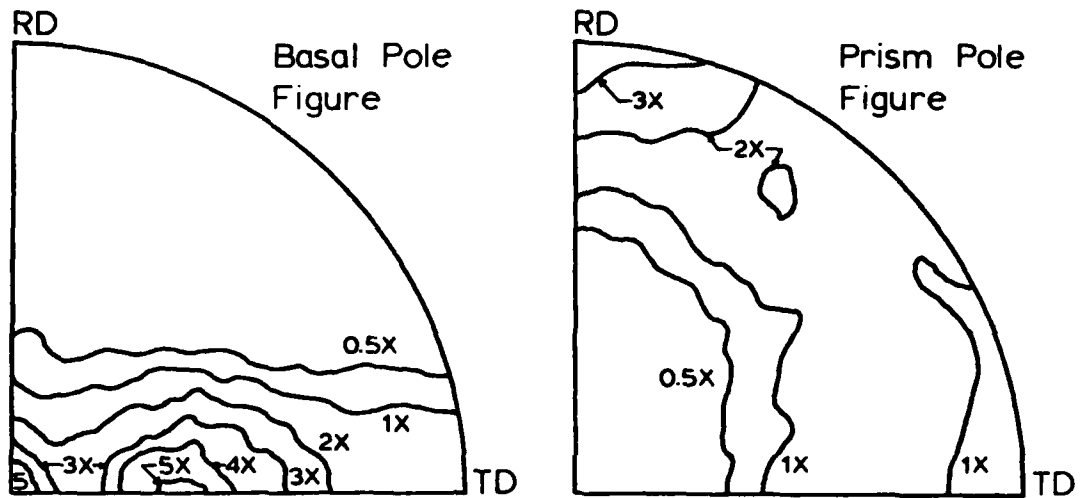


Fig. 1 - Basal and prism pole figures of the titanium sheet material tested. The numbers indicate the relative intensities of the poles in number of times random.

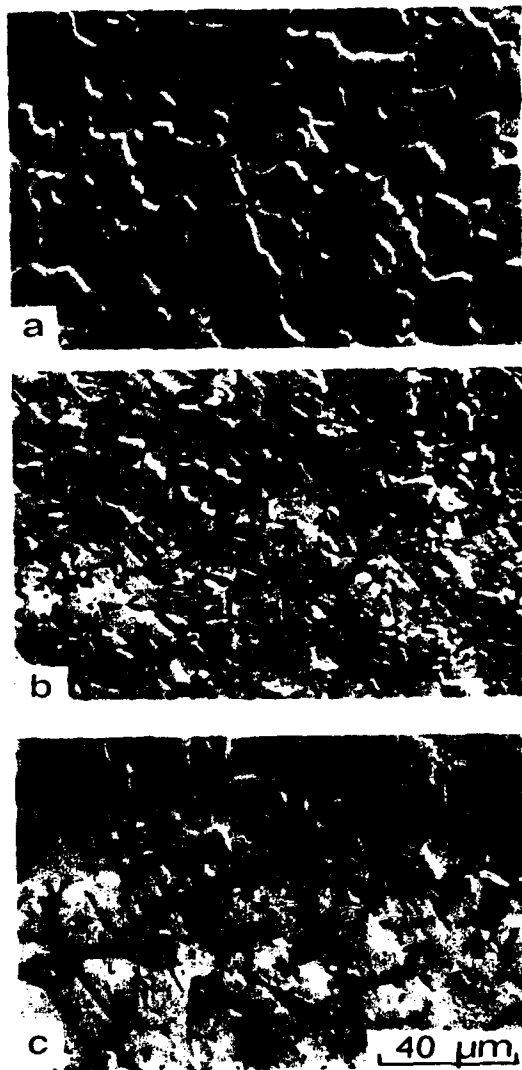


Fig. 2 - Optical micrograph showing titanium sheet containing (a) 60 ppm H, (b) 630 ppm H, and (c) 980 ppm H.

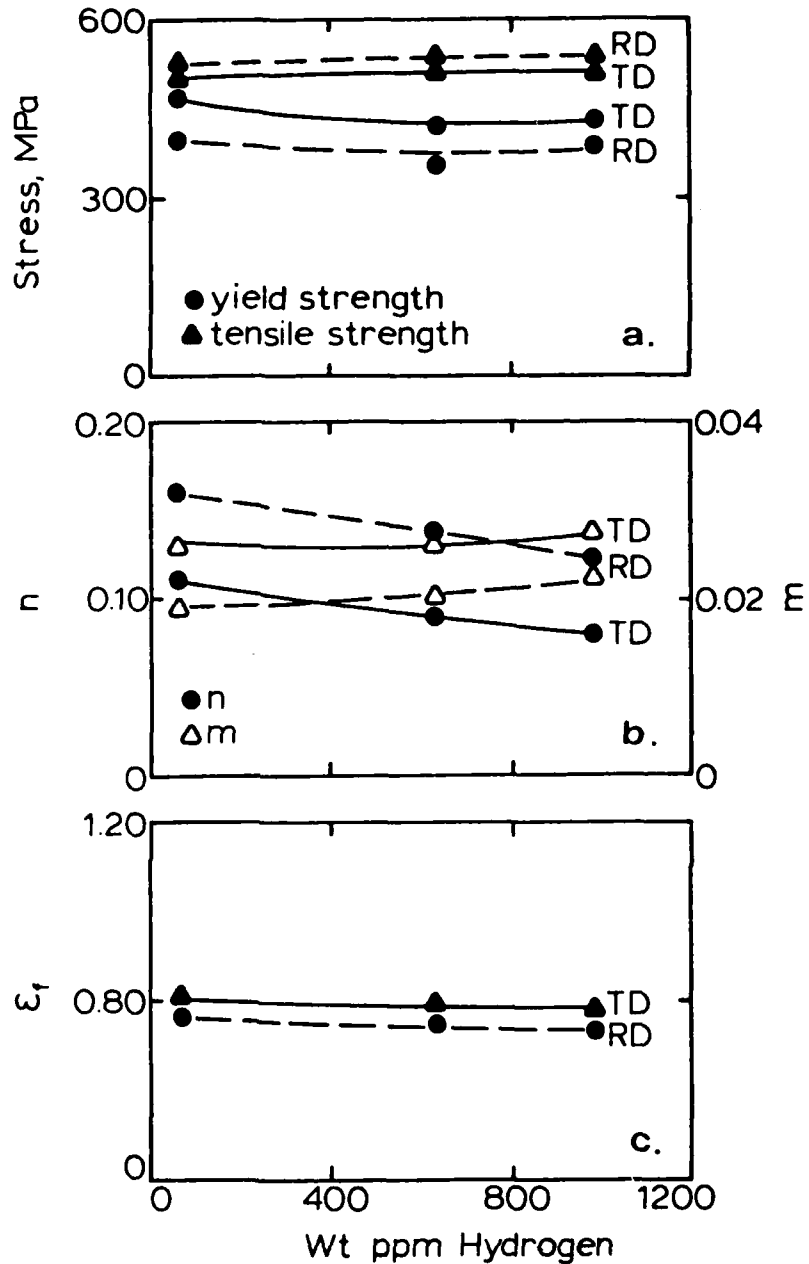


Fig. 3 - The influence of hydrogen content on the (a) yield and tensile strength, (b) strain hardening exponent m , and strain-rate hardening exponent, m , and (c) the local fracture strain. All data are from uniaxial tensile tests of specimens either parallel to the rolling direction RD or transverse to the rolling direction TD.

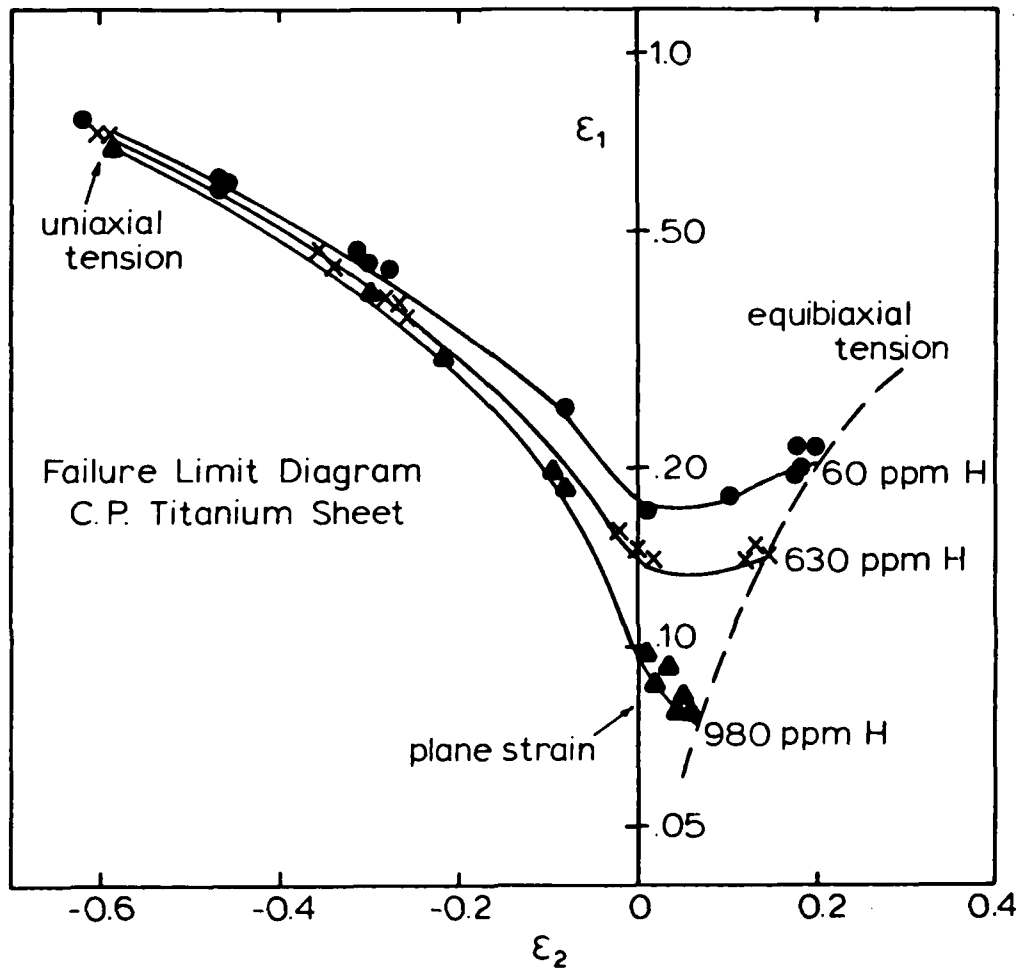


Fig. 4 - A fracture limit diagram showing the major ϵ_1 and minor ϵ_2 principal strains in the plane of the sheet at fracture. Data is for Ti containing three levels of hydrogen and tested over a range of deformation paths.

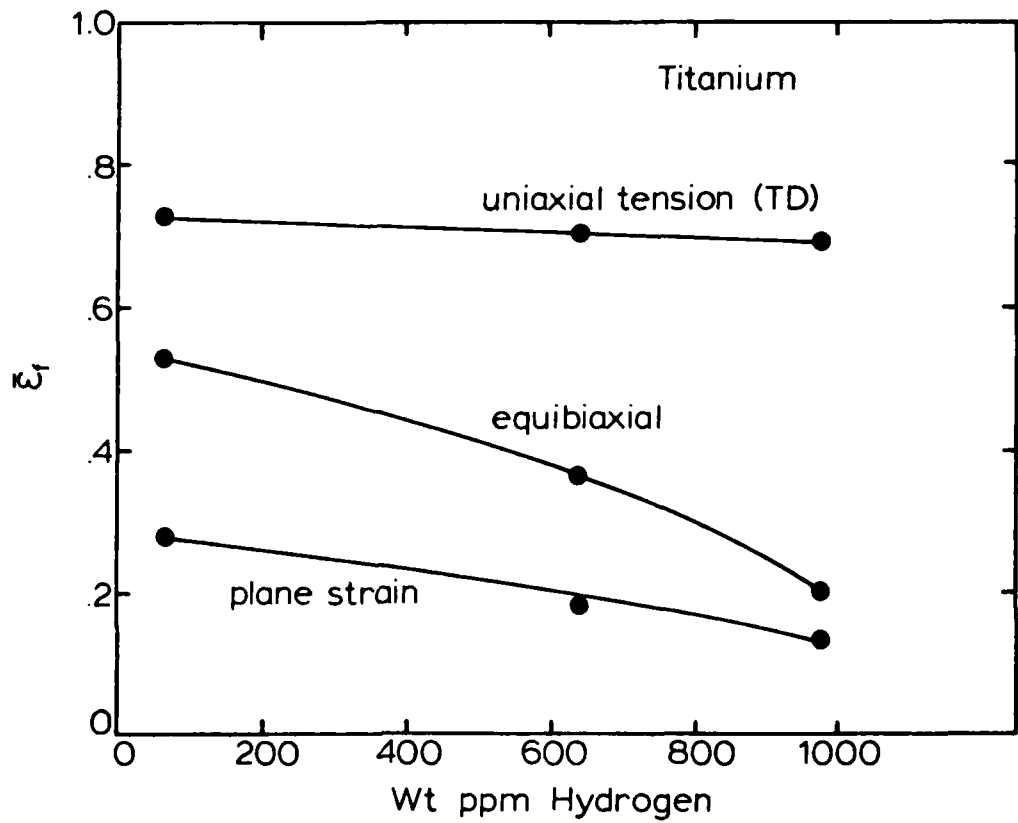


Fig. 5 - The influence of hydrogen content on the equivalent strain at fracture ϵ_f of titanium deforming in either uniaxial tension (transverse to the rolling direction), equibiaxial tension, or plane strain tension.



Fig. 6 - Electron micrographs showing strain-induced hydride fracture and void formation in (a) uniaxial tension and (b) equibiaxial tension.

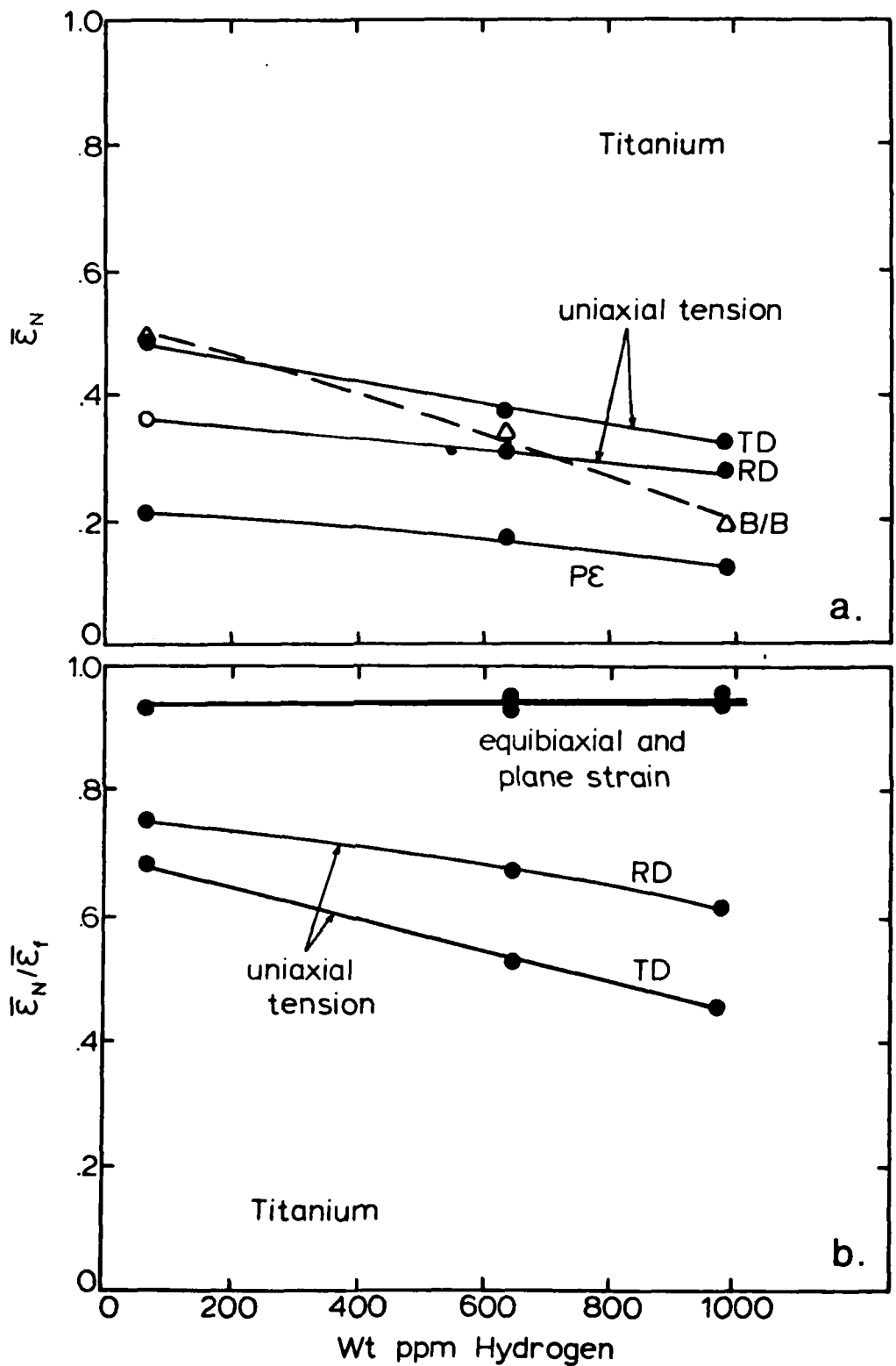


Fig. 7 - The influence of hydrogen on (a) the equivalent strain $\bar{\epsilon}_N$ required to form 10^2 voids/mm² and (b) ratio of $\bar{\epsilon}_N$ to the equivalent strain at fracture $\bar{\epsilon}_f$. The terms TD and RD refer to uniaxial tensile deformation in the transverse and rolling directions, respectively while B/B and P denote balanced biaxial and plane strain tension, respectively.

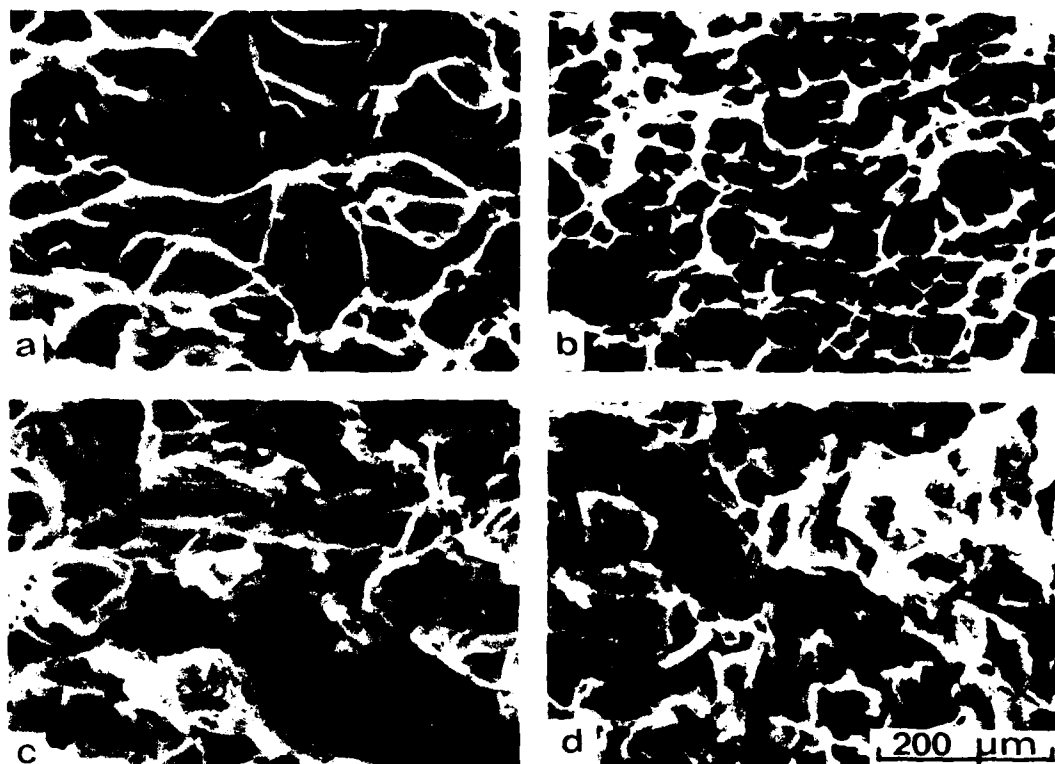


Fig. 8 - Electron micrographs showing the fracture surfaces the following specimens: (a) Ti-60 H deformed in uniaxial tension, (b) Ti-60 H deformed in equibiaxial tension, (c) Ti-980 H deformed in uniaxial tension, and (d) Ti-980 H deformed in equibiaxial tension.

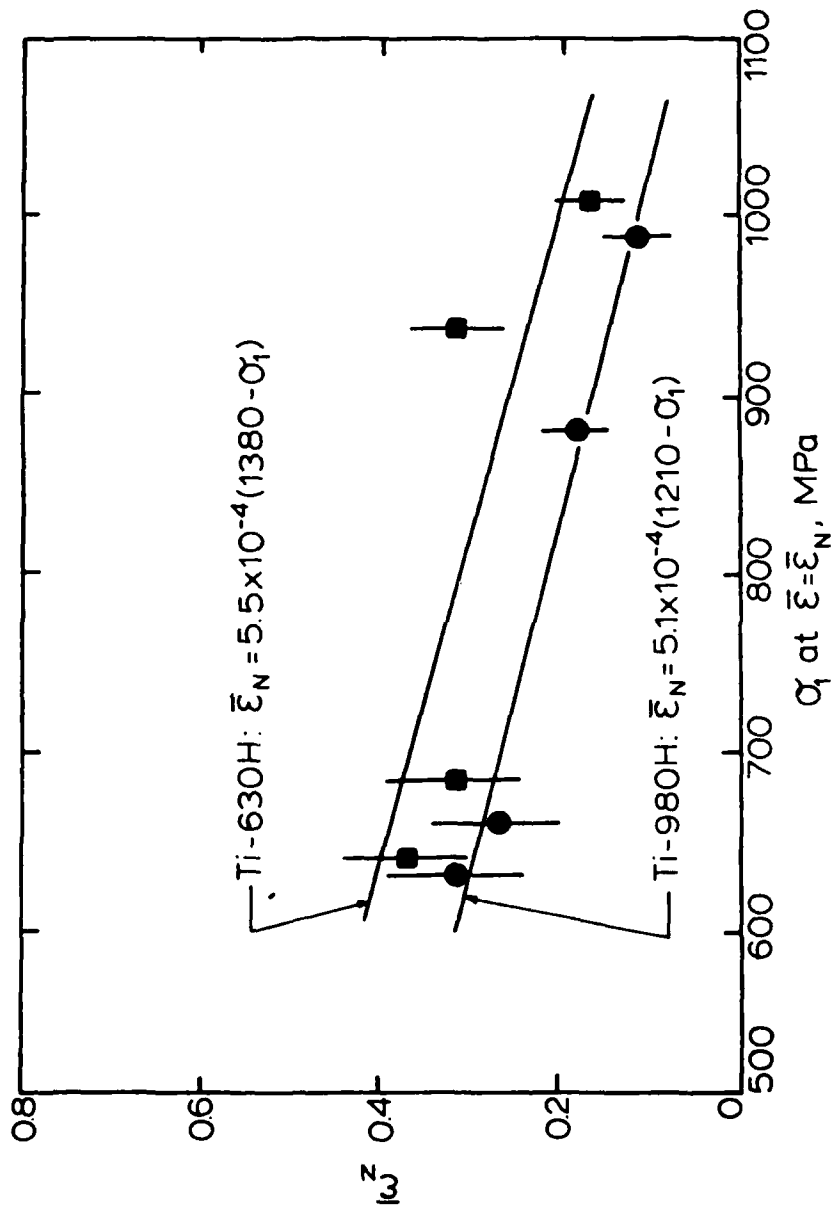


Fig. 9 - The dependence of the void nucleation strain $\bar{\epsilon}_N$ on the maximum principal stress σ_1 within the matrix at a plastic strain $\bar{\epsilon} = \bar{\epsilon}_N$.

**DA
FILM**